J|A|C|S
ARTICLES
Published on Web 04/29/2006

Self-Assembly, Structural, and Retrostructural Analysis of Dendritic Dipeptide Pores Undergoing Reversible Circular to Elliptical Shape Change

Mihai Peterca,[‡] Virgil Percec,*[,†] Andrés E. Dulcey,[†] Sami Nummelin,[†] Stephanie Korey,[†] Monica Ilies,[†] and Paul A. Heiney[‡]

Contribution from the Roy & Diana Vagelos Laboratories, Department of Chemistry, University of Pennsylvania, Philadelphia, Pennsylvania 19104-6323, and Department of Physics and Astronomy, University of Pennsylvania, Philadelphia, Pennsylvania 19104-6396

Received February 19, 2006; E-mail: percec@sas.upenn.edu

Abstract: The synthesis of dendritic dipeptides (4-3,4-3,5-4)12G2-CH_2-Boc-L-Tyr-L-Ala-OMe and (4-3, 4-3,5-4)12G2-CH_2-Boc-D-Tyr-D-Ala-OMe is described. These dendritic dipeptides self-assemble into porous elliptical and circular columns that in turn self-organize into centered rectangular columnar and hexagonal columnar periodic arrays. The transition from porous elliptical to porous circular columns is mediated in a reversible or irreversible way by the thermal history of the sample. A method to determine the dimensions of hollow elliptical and circular columns by the reconstruction of the small-angle powder X-ray diffractograms of the centered rectangular or hexagonal columnar lattices was elaborated. This technique together with wide-angle X-ray experiments performed on aligned fibers provided access to the structural and retrostructural analysis of elliptical supramolecular pores. This procedure is general and can be adapted for the determination of the dimensions of pores of any columnar shape.

Introduction

Natural pore-forming proteins and their remodeled structures exhibit a diversity of biological and biologically inspired functions such as transmembrane channels,[1] viral helical coats,[2] reversible encapsulation,[3] stochastic sensing,[4] and patogenic[5] and antibiotic activity.[6] Natural porous proteins are stable in solution and in solid state. Various synthetic strategies to porous and tubular supramolecular assemblies have been elaborated.[7] However, with few exceptions,[8] porous protein mimics do not assemble into periodically ordered structures that are stable in solution and in solid state. This behavior limits their structural analysis by combinations of solution and solid state complementary techniques. Our laboratory reported the self-assembly of amphiphilic dendritic dipeptides to produce helical pores that are stable both in solution and in solid state.[9] For the same dendron and dipeptide, the internal structure and stability of the pore are programmed by the stereochemistry[10a] and the protective groups[10b] of the dipeptide and by the number of the methylenic units in the alkyl groups attached to the periphery of the dendron.[10c] This process is cooperative and involves allosteric regulation.[11] The same principles may apply to the self-assembly of dendritic dipeptides based on different dendrons[12] and dipeptides.

[†] Roy & Diana Vagelos Laboratories, Department of Chemistry, University of Pennsylvania.

[‡] Department of Physics and Astronomy, University of Pennsylvania.

(1) (a) MacKinnon, *R. Angew. Chem., Int. Ed.* **2004**, *43*, 4265−4277. (b) Agre, P. *Angew. Chem., Int. Ed.* **2004**, *43*, 4278−4290.
(2) (a) Klug, A. *Angew. Chem., Int. Ed. Engl.* **1983**, *22*, 565−582. (b) Klug, A. *Philos. Trans. R. Soc. London, Ser. B* **1999**, *354*, 531−535.
(3) Ishii, D.; Kinbara, K.; Ishida, Y.; Ishii, N.; Okochi, M.; Yohda, M.; Aida, T. *Nature* **2003**, *423*, 628−632.
(4) Bayley, H.; Cremer, P. S. *Nature* **2001**, *413*, 226−230.
(5) Gouaux, E. *J. Struct. Biol.* **1998**, *121*, 110−122.
(6) Wallace, B. A. *Biophys. J.* **1986**, *49*, 295−306.
(7) (a) Nolte, R. J. M.; van Beijnen, A. J. M.; Neevel, J. G.; Zwikker, J. W.; Verkley, A. J.; Drenth, W. *Isr. J. Chem.* **1984**, *24*, 297−301. (b) Jullien, L.; Lehn, J.-M. *Tetrahedron Lett.* **1988**, *29*, 3803−3806. (c) Cross, G. G.; Fyles, T. M.; James, T. D.; Zojaji, M. *Synlett* **1993**, *7*, 449−460. (d) Gokel, G. W.; Ferdani, R.; Liu, J.; Pajewski, R.; Shabany, H.; Uetrecht, P. *Chem.—Eur. J.* **2001**, *7*, 33−39. (e) Bong, D. T.; Clark, T. D.; Granja, J. R.; Ghadiri, M. R. *Angew. Chem., Int. Ed.* **2001**, *40*, 988−1011. (f) Sakai, N.; Mareda, J.; Matile, S. *Acc. Chem. Res.* **2005**, *38*, 79−87. (g) Rosselli, S.; Ramminger, A.-D.; Wagner, T.; Silier, B.; Wiegand, S.; Häussler, W.; Lieser, G.; Scheumann, V.; Höger, S. *Angew. Chem., Int. Ed.* **2001**, *40*, 3138−3141. (h) Hill, D. J.; Mio, M. J.; Prince, R. B.; Hughes, T. S.; Moore, J. S. *Chem. Rev.* **2001**, *101*, 3893−4012. (i) Fenniri, H.; Deng, B.-L.; Ribbe, A. E. *J. Am. Chem. Soc.* **2002**, *124*, 11064−11072. (j) Hecht, S.; Khan, A. *Angew. Chem., Int. Ed.* **2003**, *42*, 6021−6024. (k) Couet, J.; Jeyaprakash, J. D.; Samuel, S.; Kopyshev, A.; Santer, S.; Biesalski, M. *Angew. Chem., Int. Ed.* **2005**, *44*, 3297−3301.
(8) (a) Ghadiri, M. R.; Granja, J. R.; Milligan, R. A.; McRee, D. E.; Khazanovich, N. *Nature* **1993**, *366*, 324−327. (b) Petitjean, A.; Cuccia, L. A.; Lehn, J.-M.; Nierengarten, H.; Schmutz, M. *Angew. Chem., Int. Ed.* **2002**, *41*, 1195−1198. (c) Ohkita, M.; Lehn, J.-M.; Baum, G.; Fenske, D. *Chem.—Eur. J.* **1999**, *5*, 3471−3481. (d) Schmitt, J.-L.; Stadler, A.-M.; Kyritsakas, N.; Lehn, J.-M. *Helv. Chim. Acta* **2003**, *86*, 1598−1624. (e) Schmitt, J.-L.; Lehn, J.-M. *Helv. Chim. Acta* **2003**, *86*, 3417−3426.
(9) (a) Percec, V.; Dulcey, A. E.; Balagurusamy, V. S. K.; Miura, Y.; Smidrkal, J.; Peterca, M.; Nummelin, S.; Edlund, U.; Hudson, S. D.; Heiney, P. A.; Duan, H.; Magonov, S. N.; Vinogradov, S. A. *Nature* **2004**, *430*, 764−768. (b) Rouhi, M. *Chem. Eng. News* **2004**, *82* (33), 4. (c) Borman, S. *Chem. Eng. News* **2004**, *82* (51), 53−61.
(10) (a) Percec, V.; Dulcey, A. E.; Peterca, M.; Ilies, M.; Ladislaw, J.; Rosen, B. M.; Edlund, U.; Heiney, P. A. *Angew. Chem., Int. Ed.* **2005**, *44*, 6516−6521. (b) Percec, V.; Dulcey, A. E.; Peterca, M.; Ilies, M.; Sienkowska, M. J.; Heiney, P. A. *J. Am. Chem. Soc.* **2005**, *127*, 17902−17909. (c) Percec, V.; Dulcey, A. E.; Peterca, M.; Ilies, M.; Nummelin, S.; Sienkowska, M. J.; Heiney, P. A. *Proc. Natl. Acad. Sci. U.S.A* **2006**, *103*, 2518−2523.
(11) (a) Monod, J.; Changeux, J.-P.; Jacob, F. *J. Mol. Biol.* **1963**, *6*, 306−329. (b) Perutz, M. *Mechanisms of Cooperativity and Allosteric Regulation in Proteins*; Cambridge University Press: Cambridge, U.K., 1990. (c) Evans, P. R. *Curr. Opin. Struct. Biol.* **1991**, *1*, 773−779.
(12) Percec, V.; Dulcey, A. E.; Peterca, M.; Ilies, M.; Miura, Y.; Edlund, U.; Heiney, P. A. *Aust. J. Chem.* **2005**, *58*, 472−482.

Scheme 1. Synthesis of the New Dendritic Dipeptides (4-3,4-3,5-4)12G2-CH_2-X, X = Boc-L-Tyr-L-Ala-OMe and Boc-D-Tyr-D-Ala-OMe.

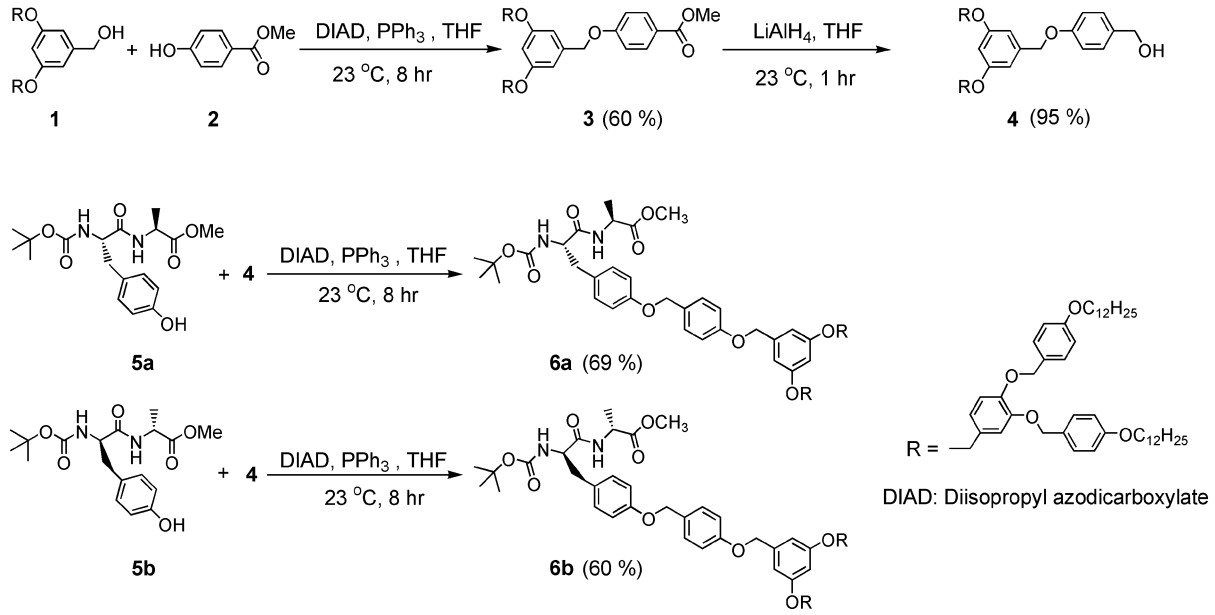

Porous structures self-assembled from dendritic dipeptides reported up to now,[9,10,12] as well as porous structures assembled from other architectures,[7,8] have a circular shape of the pore. Nonetheless, natural pore-forming proteins display also other pore shapes. A representative example is the hourglass shape of aquaporin.[1b] Currently we are searching through libraries of supramolecular porous structures forming lattices that have the potential to indicate strategies to noncircular pore shapes. Preliminary reports[10c,13] have indicated the possibility of generating elliptical pores from several dendritic alcohols that were used as precursors to dendritic dipeptides. However, their *c*2*mm* centered rectangular columnar (Φ_{r-c}) lattice exhibited a small number of X-ray diffraction peaks resulting in low spatial resolution. In addition, structural and retrostructural analysis methods for supramolecular pores were available only for structures with circular shape.[9]

We now report the synthesis of dendritic dipeptides that self-assemble into circular pores which, depending on their kinetic treatment and on the degree of order of the pore, undergo either reversible or irreversible circular-to-elliptical shape changes. A combination of electron density maps together with the reconstruction of their small-angle and wide-angle X-ray diffraction (XRD) experiments performed on powder and oriented fibers combined with experimental densities was used to develop methods for the structural and retrostructural analysis of elliptical pores.

Results and Discussion

Synthesis of (4-3,4-3,5-4)12G2-CH_2-Boc-L-Tyr-L-Ala-OMe and (4-3,4-3,5-4)12G2-CH_2-Boc-D-Tyr-D-Ala-OMe. The second generation dendron (4-3,4-3,5)12G2-CH_2OH (**1**) synthesized as reported previously[9,14] was etherified with **2** under Mitsunobu reaction conditions[15] to produce (4-3,4-3,5-4)12G2-CO_2CH_3 (**3**) (60% yield) (Scheme 1). Reduction of **3** with $LiAlH_4$ in THF yielded (4-3,4-3,5-4)12G2-CH_2OH (**4**) (95% yield). Mitsunobu etherification of Boc-L-Tyr-L-Ala-OMe (**5a**)[9] and Boc-D-Tyr-D-Ala-OMe (**5b**)[9] with **4** generated the enantiomeric dendritic dipeptides (4-3,4-3,5-4)12G2-CH_2-Boc-L-Tyr-L-Ala-OMe (**6a**) (69%) and (4-3,4-3,5-4)12G2-CH_2-Boc-D-Tyr-D-Ala-OMe (**6b**) (60%). A combination of ^1H and ^{13}C NMR, HPLC, and MALDI-TOF techniques was used to demonstrate the structure and purity (>99%) of all intermediary and final compounds.

Structural Analysis of the Supramolecular Assemblies. The structural analysis of the supramolecular porous assemblies generated from these dendritic dipeptides was carried out by a combination of differential scanning calorimetry (DSC) and small- and wide-angle powder and fiber XRD experiments. The strategy employed is outlined below.

The porous structure of the columns was identified by the enhanced intensity of the higher order XRD diffractions and was visualized by the reconstructed electron density maps calculated from the XRD data.[9a,10] The size of the elliptical pore was determined by elaborating a method for the reconstruction of the XRD peak positions and intensities using the electron density of the dendritic dipeptide and considering a three-phase intracolumnar model consisting of aliphatic, aromatic, and dipeptide regions and a hollow center of the column, as suggested by the electron density map. This strategy is similar to that elaborated for circular porous columns.[9a]

Transition temperatures and their enthalpy changes were obtained by DSC, and the phases associated with these transitions were assigned by XRD. The DSC analysis of the as prepared (4-3,4-3,5-4)12G2-CH_2-Boc-L-Tyr-L-Ala-OMe and (4-3,4-3,5-4)12G2-CH_2-Boc-D-Tyr-D-Ala-OMe show that they are already assembled into supramolecular columns (Figure 1).

On cooling from the isotropic state both dendritic dipeptides are self-assembled into columns that self-organize into a monotropic hexagonal columnar phase (Φ_h), followed by an enatiotropic *c*2*mm* centered rectangular columnar lattice with intracolumnar order (Φ_{r-c}^{io}). On heating, at 83 °C the Φ_{r-c}^{io} lattice undergoes a transition to a *p*6*mm* hexagonal columnar

(13) Percec, V.; Peterca, M.; Sienkowska, M. J.; Ilies, M. A.; Aqad, E.; Smidrkal, J.; Heiney, P. A. *J. Am. Chem. Soc.* **2006**, *128*, 3324−3334.
(14) (a) Percec, V.; Cho, W.-D.; Ungar, G.; Yeardley, D. J. P. *J. Am. Chem. Soc.* **2001**, *123*, 1302−1315. (b) Percec, V.; Mitchell, C. M.; Cho, W.-D.; Uchida, S.; Glodde, M.; Ungar, G.; Zeng, X.; Liu, Y.; Balagurusamy, V. S. K.; Heiney, P. A. *J. Am. Chem. Soc.* **2004**, *126*, 6078−6094.
(15) Mitsunobu, O. *Synthesis* **1981**, 1−28.

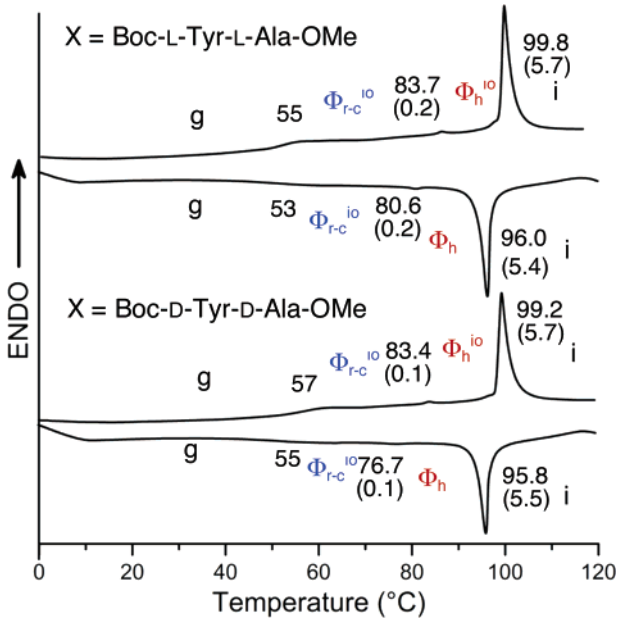

Figure 1. Second heating and cooling DSC scans (10 °C/min) of (4-3,4-3,5-4)12G2-CH_2-X; X = Boc-L-Tyr-L-Ala-OMe, Boc-D-Tyr-D-Ala-OMe. Transition temperatures (°C) and enthalpies changes (kcal/mol, in parentheses) are indicated. Φ_{r-c}^{io} = centered rectangular columnar phase with intracolumnar order; Φ_h = hexagonal columnar phase; Φ_h^{io} = hexagonal columnar phase with intracolumnar order; g = glass; i = isotropic liquid. First heating scans (not shown) are identical with the second heating scans.

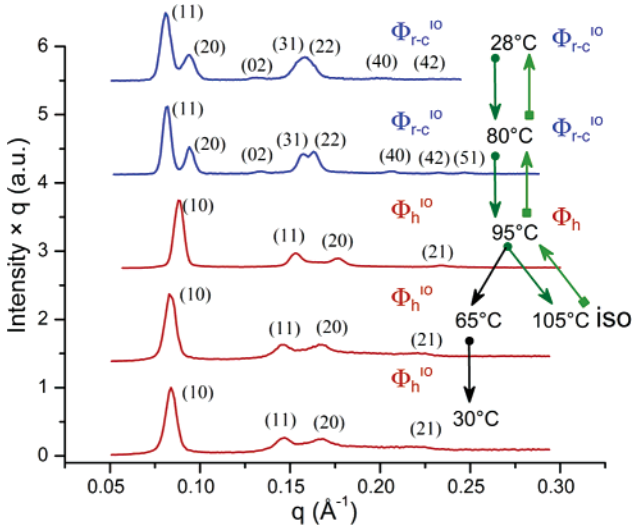

Figure 2. Small-angle X-ray diffraction plots recorded at various temperatures in the supramolecular columnar structures self-assembled from (4-3,4-3,5-4)12G2-CH_2-Boc-L-Tyr-L-Ala-OMe. Below the isotropisation temperature, the freezing of the higher order Φ_h^{io} phase is observed (see also Figure 3). Φ_{r-c}^{io} = centered rectangular columnar phase; Φ_h = hexagonal columnar phase, Φ_h^{io} = hexagonal columnar phase with intracolumnar order; $q = (4\pi/\lambda)\sin\theta$ = momentum transfer; a.u. = arbitrary units. The sequence of dark (on heating) and light (on cooling) green arrows shows the reversible $\Phi_{r-c}^{io}-\Phi_h^{io}-$isotropic$-\Phi_h-\Phi_{r-c}^{io}$ transition, while the sequence of dark green up to 95 °C and black arrows shows the irreversible $\Phi_{r-c}^{io}-\Phi_h^{io}$ transition.

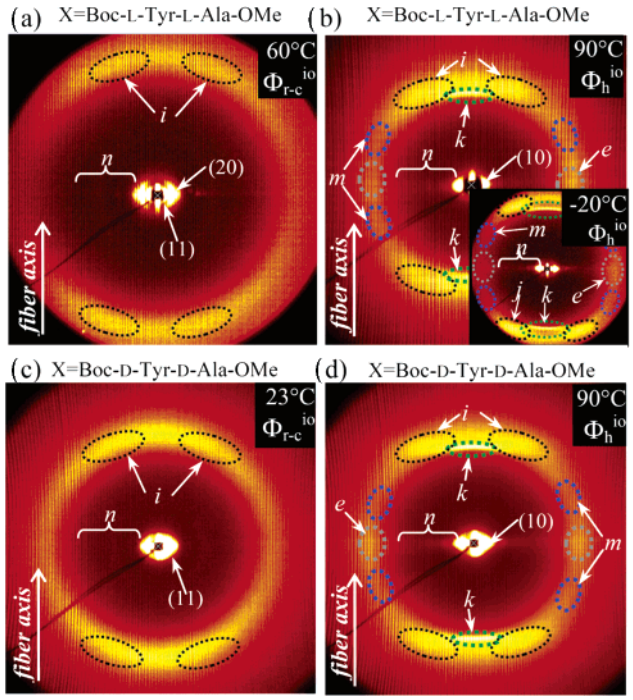

Figure 3. Wide-angle X-ray diffraction patterns recorded at the temperatures indicated in the figure on aligned fibers of (4-3,4-3,5-4)-12G2-CH_2-X. (a and b) X = Boc-L-Tyr-L-Ala-OMe; (a) in Φ_{r-c}^{io}, (b) in Φ_h^{io}; (c and d) X = Boc-D-Tyr-D-Ala-OMe; (c) in Φ_{r-c}^{io}, (d) in Φ_h^{io}; *i*, *j* = short-range features arising from helical intracolumnar order (4.6 Å for *i* and 5.0 Å for *j*); *e* = strong equatorial feature (4.8 Å); *k* = diffraction pattern features corresponding to 5.0 Å stacking of the aromatic rings along the column axis (the estimated correlation length is ~60 layers); *m* = dendron tilt (62 ± 8°); *n* = high order (*hk*0) reflections.

phase with intracolumnar order (Φ_h^{io}).[10b,c] The short-range intracolumnar order of the Φ_{r-c}^{io} and Φ_h^{io} phases was established by using wide-angle XRD experiments carried out on both powder and aligned fibers. These experiments will be discussed later. At about 99 °C the Φ_h^{io} lattices of both dendritic dipeptides transform into an isotropic liquid that is generated from self-assembled columns as demonstrated by XRD (Supporting Information, Figure SF1). The sequences of heating and cooling illustrated in Figure 1 provide strategies for the reversible and irreversible interconversion between the circular columns that assemble in the Φ_h^{io} phase and the elliptical columns that assemble in the Φ_{r-c}^{io} phase. The identification of the Φ_{r-c}^{io} and Φ_h^{io} phases was accomplished by small-angle powder XRD experiments (Figure 2 and Supporting Information, Figure SF1). When the sample was heated from 20 °C up to the isotropic phase and back, the sequence of phases from Figure 1 was reproducible (Supporting Information, Figure SF1). However, when the sample was heated only up to the Φ_h^{io} phase (95 °C) and cooled to 30 °C, the Φ_{r-c}^{io} phase was not regenerated (Figure 2). The existence of intermediate range intracolumnar order (io)[10b,c] in the supramolecular columns forming the Φ_{r-c}^{io} and Φ_h^{io} phases was established by wide-angle XRD experiments carried out on powder and on aligned fibers (Figures 3 and 4). The Φ_{r-c}^{io} and Φ_h^{io} phases exhibit a 5.0 Å stacking of the aromatic rings (Figure 4). The Φ_h^{io} phase exhibits a correlation length of about 60 layers (k), and a 62° tilt of the dendrons with respect to the column axis. The io of the hexagonal phase was identified by the presence of short-range helicity and tilt, and by the longer range registry features. The helical structure of the columns was also supported by circular dichroism experiments (Supporting Information Figure SF9).

Mechanism of the Reversibility of the Elliptical to Circular Shape Change. The reversibility vs irreversibility of the transition from elliptic to circular columns was investigated by a combination of DSC and XRD experiments. Figure 1 shows

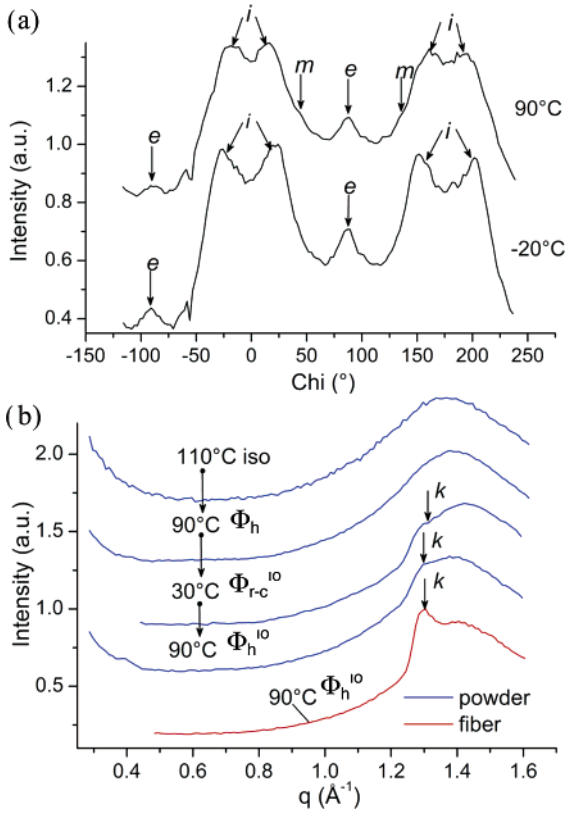

Figure 4. Chi plot of the X-ray diffraction fiber pattern shown in Figure 3b (a); (4-3,4-3,5-4)12G2CH$_2$Boc-L-Tyr-L-Ala-OMe powder and fiber q-plots at the indicated temperatures (b). Legend: i = short-range features arising from helical intracolumnar order (4.6 Å); e = strong equatorial feature (4.8 Å); m = dendron tilt; k = diffraction pattern features corresponding to 5.0 Å stacking of the aromatic rings along the column axis (the estimated correlation length is ~60 layers).

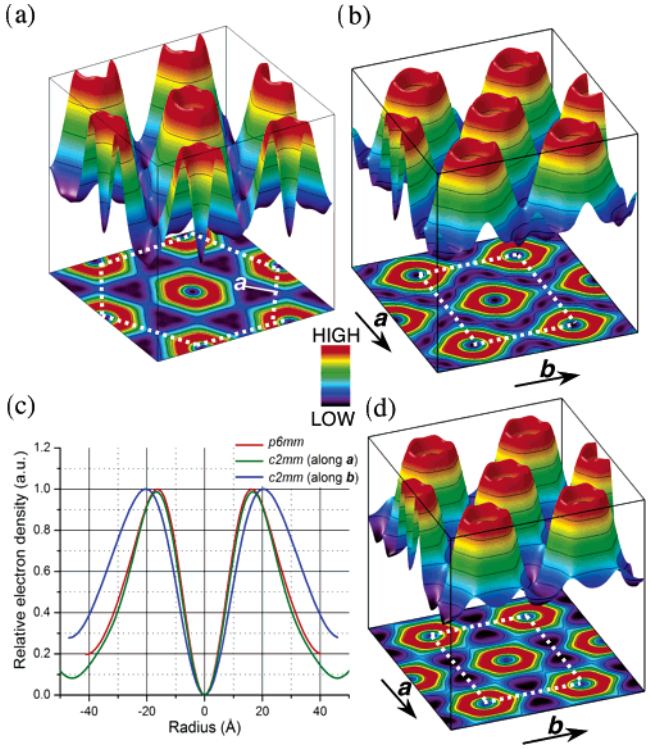

Figure 5. Reconstructed electron density maps for the lattices generated from (4-3,4-3,5-4)12G2-CH$_2$-Boc-L-Tyr-L-Ala-OMe: (a) hollow Φ_h^{io} calculated using experimental diffraction amplitudes; (b) hollow Φ_{r-c}^{io} using experimental diffraction amplitudes; (c) plot of the relative electron densities profiles as a function of column radius for the two phases; (d) hollow Φ_{r-c}^{io} generated from calculated diffraction amplitudes given by the three-level model.

the second heating and cooling DSC scans of both dendritic dipeptides. The first, second, and subsequent heating and cooling DSC scans are identical. A DSC analysis of this sequence, which consists of heating to Φ_h^{io}, annealing in the Φ_h^{io} phase for at least 5 min, cooling to 20 °C, and reheating to isotropic liquid does not show the Φ_h^{io} to Φ_{r-c}^{io} transition on cooling and reheating (Figure 2). The very small supercooling of all transition temperatures and their associated enthalpy changes demonstrate reversible and thermodynamically controlled transitions to the Φ_{r-c}^{io}, Φ_h^{io}, and Φ_h phases when the sample was heated from 20 °C to isotropic and back with 20, 10, and 5 °C/min, with a higher isotropization enthalpy at the lowest heating rate only. However, when the sample was heated to the Φ_h^{io} phase, maintained for 5 min in this phase, cooled to 20 °C, and then reheated, only the Φ_h^{io} phase was observed. An increase of 60% in the enthalpy change associated with the Φ_h^{io} to isotropic phase transition was observed under these conditions. Without annealing, the isotropization enthalpy change is 5.4 kcal/mol (Figure 1), and after annealing in the Φ_h^{io} phase, it is 8.7 kcal/mol. This substantial increase in the Φ_h^{io} to i enthalpy change demonstrates an enhancement in the order of the Φ_h^{io} phase that most probably approaches 3-D hexagonal crystal order. Annealing for more than 5 min in the Φ_h^{io} phase results in a further increase in the enthalpy change associated with the Φ_h^{io} − i transition. Annealing in the Φ_{r-c}^{io} phase does not increase the order of the phase. This is due to a very slow dynamic in the Φ_{r-c}^{io} phase that is induced by its close proximity to glass transition (Tg). Therefore, only the transition from Φ_h^{io} to isotropic liquid is kinetically controlled. This analysis explains the mechanism of the reversible Φ_h to Φ_{r-c}^{io} and Φ_{r-c}^{io} to Φ_h^{io} and of the irreversible transition from Φ_h^{io} to Φ_{r-c}^{io} phases. During the second and subsequent heating and cooling scans from 20 °C to isotropic liquid the order in the Φ_{r-c}^{io} phase is higher than that in the less ordered Φ_h and of unannealed Φ_h^{io} phases, and this provides a mechanism for the reversibility of the process. However, upon annealing, the order of the Φ_h^{io} phase becomes higher than that of the Φ_{r-c}^{io} phase. Subsequently, the formation of the Φ_{r-c}^{io} phase from the higher order Φ_h^{io} on cooling becomes thermodynamically inhibited. This trend is in agreement with thermodynamic schemes reported previously.[16] This thermal analysis clarifies the sequence discovered by the XRD experiments that is presented in Figure 2.

Reconstruction of Electron Density Maps of Columnar Hexagonal and Columnar Rectangular Lattices. Electron density maps[9,17] were reconstructed from the peak amplitudes from small-angle powder XRD of the Φ_h^{io} (Figure 5a) and Φ_{r-c}^{io} (Figure 5b) lattices. The Φ_h^{io} phase exhibits seven diffraction peaks, and the Φ_{r-c}^{io} phase shows 10 diffraction peaks. All of them were used in the calculation of the electron density maps. All possible phase choices for the X-ray diffraction amplitudes of the Φ_{r-c}^{io} phase were investigated. The solution proposed here was based on the match of the electron

(16) Percec, V.; Keller, A. *Macromolecules* **1990**, *23*, 4347−4350.
(17) Balagurusamy, V. S. K.; Ungar, G.; Percec, V.; Johansson, G. *J. Am. Chem. Soc.* **1997**, *119*, 1539−1555.

density distribution of the Φ_{r-c}^{io} phase with that of the Φ_h^{io} phase. In both cases the electron-density maps show that the dendrons self-assemble into hollow columns. These columns are circular in the case of Φ_h^{io} and elliptical in the case of Φ_{r-c}^{io}. As shown in Figure 5b, the elliptical columns are aligned with the long axis of their cross-section along the *b* axis of the Φ_{r-c}^{io} lattice. The color code shows high electron density surrounding the low electron density hollow center. The high electron density (marked in red) is generated by the dipeptide and the aromatic parts of the dendron which are considered to constitute a single microphase. The periphery of the column has low electron density that is generated by the aliphatic part of the dendron, and is highlighted in green and blue. The sharp separation among the pore, dipeptide plus aromatic, and aliphatic regions indicates a three-phase microsegregated structure in the supramolecular column (Figure 5a,b,c). The minimum of the electron density in the center of the column is below the electron density from the aliphatic part that is located at the periphery of the column. This indicates that a pore penetrates through the center of the column.

Calculation of the Elliptical Pore Size by the Reconstruction of the XRD. The calculation of the elliptical pore size was accomplished by the reconstruction of the XRD via a least-squares fit of the observed positions and amplitudes of the diffraction peaks to those calculated based on a simplified model consisting of cylindrical or elliptical shells of constant density. The relative electron density in each shell is calculated from the molecular structure of the dendritic dipeptide, and therefore, the only fitting parameters are the shell radii. This approach was used previously to reconstruct the lyotropic hexagonal phase generated from lipids[18] and the circular porous hexagonal phase reported from our laboratory.[9a] Figure 7 outlines the three-level model of the elliptical and of the circular columns derived from the electron-density maps in Figure 5. The structure of the dendritic dipeptide uses the same color code as that in the supramolecular column shown in Figure 5d. The numbers of electrons in the aromatic and dipeptide (N_{arom}) and in the aliphatic (N_{aliph}) parts of the dendritic dipeptide molecule are also shown in Figure 6d. The reconstruction of the powder XRD that includes both the position and the amplitude of the XRD of the Φ_{r-c} lattice follows the principle of multilevels of constant electron density used previously.

The scattering amplitude $F(\vec{q})$ for a structure with position-dependent electron density $\rho(\vec{r})$ has the general form:[18]

$$F(\vec{q}) = \int \rho(\vec{r}) e^{i\vec{q}\vec{r}}\, d\vec{r}, \qquad i = \sqrt{-1} \tag{1}$$

For the case of the Φ_{r-c} phase, the electron density of the elliptical cylinder is

$$\rho(x,y) = \begin{cases} \rho_0 & \dfrac{x^2}{R_x^2} + \dfrac{y^2}{R_y^2} \le 1 \\ 0 & \dfrac{x^2}{R_x^2} + \dfrac{y^2}{R_y^2} > 1 \end{cases} \tag{2}$$

where ρ_0 is constant and R_x, R_y are the semiminor and semi-major axis radii, respectively (Figure 5b). Substituting eq 2 into eq 1 and performing the Fourier transform we find

$$F(q_x,q_y) = \rho_0 2\pi R_x R_y \frac{J_1\left(\sqrt{(R_x q_x)^2 + (R_y q_y)^2}\right)}{\sqrt{(R_x q_x)^2 + (R_y q_y)^2}} \tag{3}$$

To reduce the number of fitted parameters, we assume that the ellipticity ratio, defined by $\epsilon = R_x/R_y$, is identical for all three shells of the column. This is equivalent to a smooth and uniform distortion of the circular columns into elliptical columns. The complete scattering amplitude then becomes

$$F_{model}^{(c2mm)}(q_x,q_y) = F_{ellipt}(R_{aliph},\rho_{aliph}) - F_{ellipt}(R_{arom},\rho_{aliph}) + F_{ellipt}(R_{arom},\rho_{arom}) - F_{ellipt}(R_{pore},\rho_{arom}) \tag{4}$$

where

$$F_{ellipt}(R,\rho) = A2\pi\epsilon R^2 \rho \frac{J_1\left(\sqrt{(\epsilon R q_x)^2 + (R q_y)^2}\right)}{\sqrt{(\epsilon R q_x)^2 + (R q_y)^2}} \tag{5}$$

Here $q_x = 2\pi h/a$ and $q_y = 2\pi k/b$ are the Cartesian components of the momentum transfer, *a* and *b* are the dimension of the Φ_{r-c} lattice, and ρ_{aliph}, ρ_{arom}, and ρ_{pore} are the charge densities in the aliphatic, aromatic, and pore regions, respectively (units $e^-/Å^3$), calculated from the number of electrons in each region (N_{aliph}, N_{arom}, and N_{pore}) and the radii of the different regions (R_{aliph}, R_{arom}, and R_{pore}). *A* is an overall amplitude prefactor. When $\epsilon = 1$, eq 4 reduces to the equation used previously to calculate the pores size of circular porous columns[9] assembled in the Φ_h phase. The experimental XRD intensities are converted

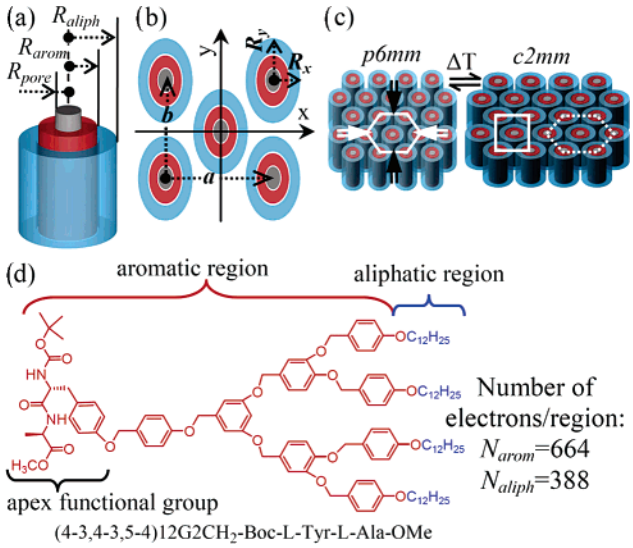

Figure 6. Three-level models of the elliptical asymmetric and of the circular symmetric columns derived from the electron density maps. (a) R_{aliph} = the aliphatic region of the column; R_{arom} = the combined peptide and aromatic region of the column; R_{pore} = the hollow region; (b) ***a***, ***b*** = *c*2*mm* lattice vectors; their orientation in the (*xy*) plane is indicated; (c) the distortion along a preferred direction of the *p*6*mm* phase generates the *c*2*mm* phase; each of the two possible directions is highlighted by black and white double arrows, respectively; (d) the structure of the dendritic dipeptide (4-3,4-3,5-4)12G2-CH$_2$-Boc-L-Tyr-L-Ala-OMe that self-assembles into porous columns; N_{arom} = number of electrons in the aromatic region; N_{aliph} = number of electrons in the aliphatic region.

(18) Turner, D. C.; Gruner, S. M. *Biochemistry* **1992**, *31*, 1340−1355.

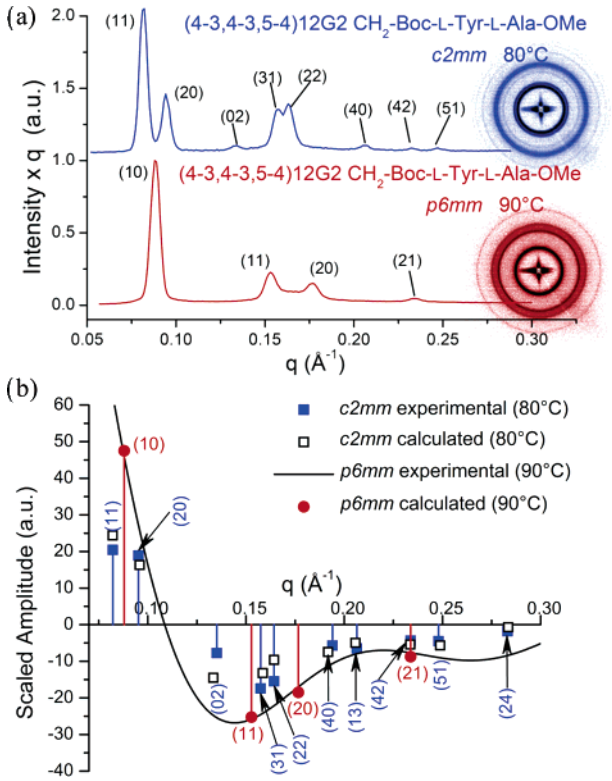

Figure 7. X-ray diffraction patterns and plots of (4-3,4-3,5-4)12G2-CH_2-Boc-L-Tyr-L-Ala-OMe (a) in the Φ_{r-c}^{io} (top) and Φ_h^{io} (bottom) phases. (b) Experimental and calculated diffraction amplitudes for the Φ_{r-c}^{io} and Φ_h^{io} phases of the supramolecular columnar assemblies generated from (4-3,4-3,5-4)12G2-CH_2-Boc-L-Tyr-L-Ala-OMe; a.u. = arbitrary units.

into scaled amplitudes after applying the appropiate multiplicity and Lorentz corrections:

$$A_{(hk)} = \frac{\sqrt{I_{hk}/q_{hk}m_{hk}}}{\sum_{(h'k')}\sqrt{I_{h'k'}/q_{h'k'}m_{h'k'}}} \qquad (6)$$

where I_{hk} is the integrated intensity of the X-ray powder peak with indices h and k, m_{hk} is the multiplicity of the peak, and the sum in the denominator is performed over all observed reflections. The experimental amplitudes were least-squares fit to the amplitudes given by eq 4 by varying the five parameters of the model: A, R_{aliph}, R_{arom}, R_{pore}, and ϵ. The phase of the amplitudes, (+- - -) for the Φ_h^{io} and (++- - - - - - - -) for the Φ_{r-c} phases from Figure 7b, were selected as described at the beginning of the previous subchapter.

Figure 7a shows XRD powder intensities of (4-3,4-3,5-4)-12G2-CH_2-Boc-L-Tyr-L-Ala-OMe in the Φ_{r-c}^{io} phase at 80 °C and in the Φ_h^{io} phase at 90 °C. A total of 7 diffraction peaks were observed in the Φ_h^{io} phase and 10 in the Φ_{r-c}^{io} phase. However, for the pore size calculation only the first 4 peaks of the Φ_h^{io} phase and all 10 of the Φ_{r-c}^{io} phase were used in the calculation. The higher order diffraction peaks of the Φ_h^{io} have a larger error in their peak area and, therefore, would introduce a large error in the pore size calculation. For the case of Φ_{r-c}^{io}, the diffraction peaks higher than 20 and, for the case of Φ_h^{io}, higher than 10 exhibit enhanced amplitudes (Figure 7a). These enhanced amplitudes provide a rapid method to screen libraries of supramolecular columns and detect porous columns. The experimental and calculated scaled amplitudes for these two lattices are plotted in Figure 7b. Details of the calculation are presented in the Supporting Information (Figures SF3 and SF5, Tables ST1 and ST2). The values of the pore diameter (D_{pore}) used to reconstruct the XRD from Figure 7b are summarized in Table 1. Note that the same three-level least-squares fit parameters were obtained whether the model was fitted to the measured intensities or the extracted amplitudes (which depend on phase), so that the final agreement does not depend on the choice of phases.

Structural and Retrostructural Analysis of the Supramolecular Pores. The reconstruction of the small-angle powder XRD allows us to calculate the column (D_{col}) and the pore (D_{pore}) diameters. However, it does not allow us to determine the 3-D arrangement of the dendrons in the porous structure. This information is obtained by combining the results of small- and wide-angle powder XRD measurements, the analysis of the aligned fiber samples by wide-angle XRD, the experimental densities, and molecular modeling.[9a] In the absence of single-crystal XRD, fiber XRD experiments generate similar structural information.[19]

Wide-angle fiber XRD patterns for the (4-3,4-3,5-4)12G2-CH_2-Boc-L-Tyr-L-Ala-OMe and (4-3,4-3,5-4)12G2-CH_2-Boc-D-Tyr-D-Ala-OMe are shown in Figures 3 and 4. They allow us to calculate the tilt angle of the dendron, the helical pitch, and the interaromatic stacking of the aromatic rings along the column axis. Molecular simulation structures that incorporate information both from the small-angle powder and wide-angle fiber XRD results are shown in Figure 8.

Structural Analysis of Other Examples of Elliptical Pores. We reported in several previous publications[10c,13] the discovery of dendrons that self-assemble into elliptical columns that self-organize in Φ_{r-c}^{io} phases exhibiting the signature of a porous elliptical column in their XRD. However, methods to calculate their pore dimensions D_{pore} were not available at that time. Therefore, we report here the structural analysis of some of these structures by using the method elaborated in the previous sections.

The precursors to dendritic dipeptides (4-3,4-3,5)12G2-CH_2OH with $n = 6$ and 8 show Φ_h^{io} and Φ_{r-c}^{io} phases, during their first heating scans, while, during their cooling and second heating scans, they exhibit Φ_{r-c}^{io} and Φ_{r-c} phases.[10c] The reconstruction of the XRD data for the Φ_h^{io} and Φ_{r-c} phases of (4-3,4-3,5)6G2-CH_2OH is detailed in the Supporting Information (Table ST4, Figure SF7 and SF8). The electron-density maps of these two structures are shown in Figure 9b,e. The column diameters D_{col} and D_{pore} along the a and b axis of the Φ_{r-c} lattice are also shown in Figure 9. For comparison, Figure 9a,d show the same data for the Φ_h^{io} and Φ_{r-c} assembled from (4-3,4-3,5-4)12G2-CH_2-Boc-L-Tyr-L-Ala-OMe. As seen in Figure 9d,e, both the elliptical pores assembled from (4-3,4-3,5-4)12G2-CH_2-Boc-L-Tyr-L-Ala-OMe and from (4-3,4-3,5)6G2-CH_2OH are deformed longitudinally along the b axis of the Φ_{r-c}^{io} lattice. Also, in both cases ϵ has almost the same value, i.e., 0.87 and 0.88, respectively.

The reconstruction of the XRD of the Φ_h^{io} and Φ_{r-c}^{io} phases of (4Pr-3,4Pr-3,5Pr)12G2-CH_2OH[13] are reported in the Sup-

(19) (a) Watson, J. D.; Crick, F. H. C. *Nature* **1953**, *171*, 737−738. (b) Wilkins, M. H. F.; Stokes, A. R.; Wilson, H. R. *Nature* **1953**, *171*, 738−740. (c) Franklin, R. E.; Gosling, R. G. *Nature* **1953**, *171*, 740−741.

Table 1. Structural and Retrostructural Analysis of Supramolecular Dendrimers Self-Assembled from (4-3,4-3,5-4)12G2-CH_2-X

compound X =	T (°C)	phase	d_{10}[a] (Å) d_{11}[c] (Å) d_{22}[d] (Å) (A^b, a.u.)	d_{11}[a] (Å) d_{20}[c] (Å) d_{13}[d] (Å) (A^b, a.u.)	d_{20}[a] (Å) d_{02}[c] (Å) d_{42}[d] (Å) (A^b, a.u.)	d_{21}[a] (Å) d_{31}[c] (Å) d_{33}[d] (Å) (A^b, a.u.)	lattice and column parameters (Å)	D_{pore} (Å)	ρ_{20}[g] (g/cm³)	μ[h]
Boc -L-Tyr-L-AlaOMe	90	Φ_h^{io}	71.4[a]	41.1[a]	35.6[a]	26.9[a]	$a = D_{col} = 82.3 \pm 0.4$	12.0 ± 1.5	1.03	11.5
			(47.51)	(25.26)	(18.49)	(8.74)				
	65	Φ_{r-c}^{io}	69.9[c]	68.8[c]	46.5[c]	41.3[c]	$a = 138.2 \pm 0.4$			12
			(22.49)	(21.81)	(7.74)	(14.38)	$b = 93.7 \pm 0.4$			
			39.0[d]	31.1[d]	27.7[d]	26.1[d]	$D_{col} = 81.6 \pm 0.4$[e]	13.9 ± 1.6[e]		
			(17.69)	(7.41)	(4.95)	(3.52)	$D_{col} = 93.8 \pm 0.4$[f]	16.0 ± 1.9[f]		
Boc -D-Tyr-D-AlaOMe	90	Φ_h^{io}	71.7[a]	41.2[a]	35.7[a]	27.0[a]	$a = D_{col} = 82.6 \pm 0.4$	11.6 ± 1.5	1.03	11.5
			(49.32)	(24.43)	(17.71)	(8.54)				
	60	Φ_{r-c}^{io}	78.1[c]	66.5[c]	48.4[c]	40.4[c]	$a = 133.5 \pm 0.4$			12
			(21.06)	(20.71)	(5.40)	(14.59)	$b = 96.5 \pm 0.4$			
			39.2[d]	31.3[d]	27.3[d]	25.69[d]	$D_{col} = 78.9 \pm 0.4$[e]	13.8 ± 1.6[e]		
			(20.08)	(6.15)	(4.85)	(4.56)	$D_{col} = 96.7 \pm 0.4$[f]	16.9 ± 2.0[f]		

[a] *d*-Spacings of the Φ_h^{io} phase. [b] Peak amplitude scaled to the sum of the observed diffraction peaks (a.u., arbitrary units). [c,d] d-Spacings of the Φ_{r-c}^{io} phase. [e] Calculated D_{col} or D_{pore} along the *a* axis of the Φ_{r-c}^{io} phase. [f] Calculated D_{col} or D_{pore} along the *b* axis of the Φ_{r-c}^{io} phase. [g] Experimental density measured at 20 °C. [h] Number of dendrons per column stratum, $\mu = (\sqrt{3}N_A D^2 t\rho)/2M$, where $N_A = 6.0220455 \times 10^{23}$ mol^{-1} is Avogadro's number, M is the molecular weight of the dendron, and $t = 5$ Å is the average height of the column stratum; Φ_h^{io} = columnar hexagonal phase with intracolumnar order; Φ_{r-c} = centered rectangular columnar phase; D_{col} = column diameter; D_{pore} = pore diameter.

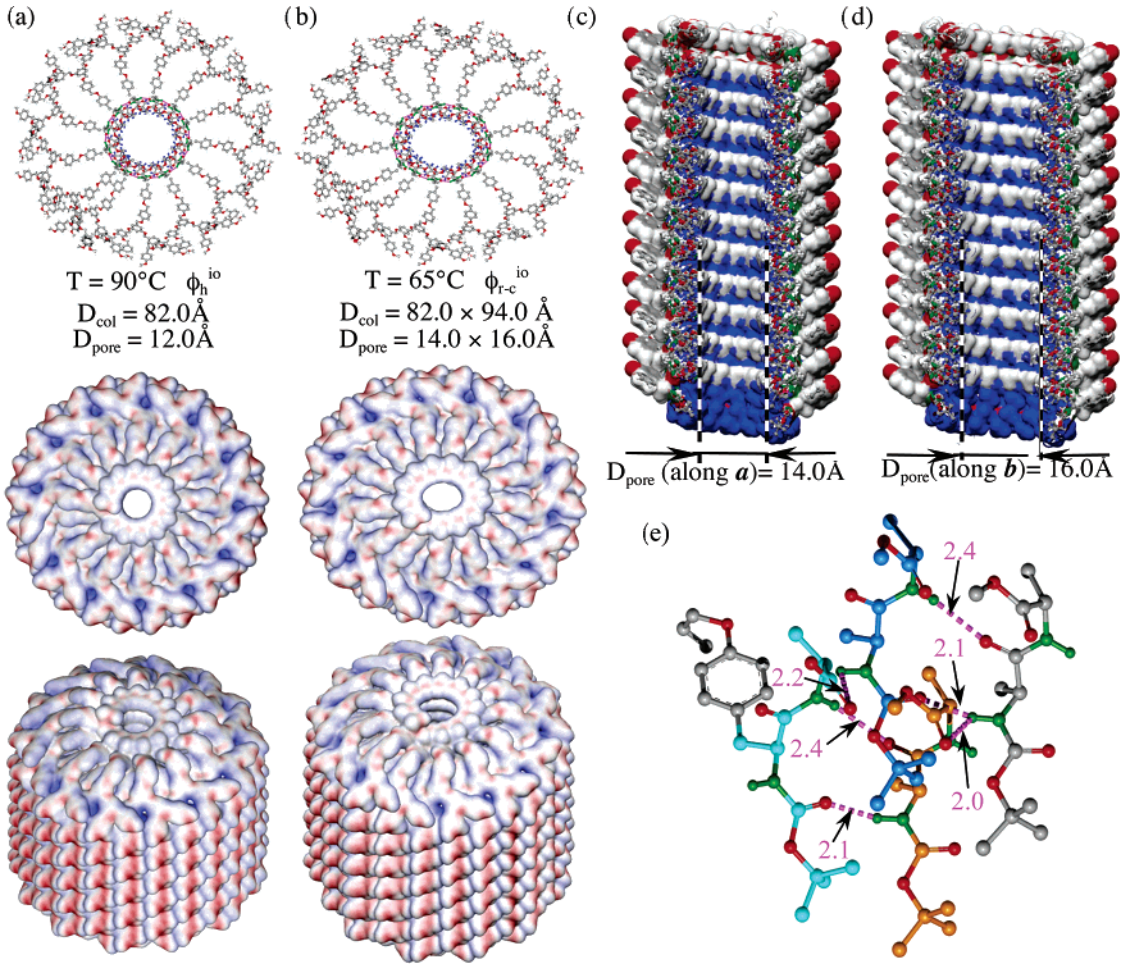

Figure 8. Supramolecular columnar assemblies generated from (4-3,4-3,5-4)12G2-CH_2-Boc-L-Tyr-L-AlaOMe. (a) Top view of one layer of the circular column, together with top and side views of the porous column in the Φ_h^{io} phase (bottom); (b) top view of one layer of the elliptical column, together with top and side views of the porous column in the Φ_{r-c}^{io} phase (bottom); (c, d) cross-sections of the porous columns from (b) along the two axis (***a*** and ***b***, respectively) of the Φ_{r-c}^{io} phase; (e) H-bonding network (in Å) between the dipeptides forming the rigid part of the pore via the mechanism described previously.[9a,10,12] Color code: $-CH_3$ from Boc protective group of Tyr, blue; $-CH_3$ of the methyl ester of Ala, white; C, gray; O, red; N−H, green. For simplicity, in (a) and (b) only the aromatic part of the dendritic dipeptides (including a methoxy group) is shown, while in (c, d, and e) only the dipeptide is shown; in (e) four dipeptides from two adjacent and interdigitated layers are illustrated with their C atoms colored differently: in the top layer the C atoms are in light blue and dark blue, respectively, while in the bottom layer one of the two dipeptides has the C atoms in gray and the other one has them in gold.

porting Information (Table ST3, Figure SF6). Their electron-density maps are shown in Figure 9c (for the Φ_h^{io} phase) and 9f (for the Φ_{r-c}^{io} phase). The D_{col} and D_{pore} data for both the symmetric and asymmetric pores are shown in Figure 9c,d.

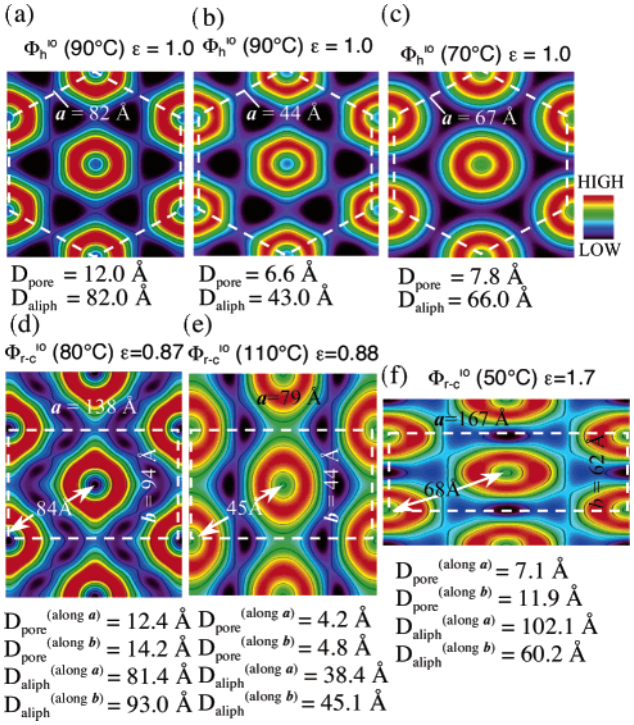

Figure 9. Reconstructed 2-D electron-density maps of porous structures assembled from (4-3,4-3,5-4)12G2-CH_2-Boc-L-Tyr-L-Ala-OMe in the Φ_h^{io} (a) and Φ_{r-c}^{io} (d) phases; from (4-3,4-3,5)6G2-CH_2OH in the Φ_h^{io} (b) and Φ_{r-c}^{io} (e) phases; and from (4Pr-3,4Pr-3,5Pr)12G2-CH_2OH in the Φ_h^{io} (c) and Φ_{r-c}^{io} (f) phases.

There is a striking difference between the elliptical pore reported in Figure 9d,e and that from Figure 9f. While in the first two cases the long axis of the pore is along the *b* axis of the Φ_{r-c} lattice, in the third case it is along the *a* axis of the lattice. Even more striking is the much larger deformation of the asymmetric pore generated from (4Pr-3,4Pr-3,5Pr)12G2-CH_2OH that has $\epsilon = 1.7$.

Conclusions

The synthesis of the dendritic dipeptides (4-3,4-3,5-4)12G2-CH_2-Boc-L-Tyr-L-Ala-OMe and (4-3,4-3,5-4)12G2-CH_2-Boc-D-Tyr-D-Ala-OMe was reported. Both dendritic dipeptides self-assemble into porous columns which in turn self-organize into Φ_{r-c}^{io} and Φ_h^{io} lattices. The columns forming the Φ_{r-c}^{io} phase have an elliptical pore shape, while those forming the Φ_h^{io} phase have a circular pore shape. Although elliptical columns forming thermotropic Φ_{r-c} liquid crystal phases are known,[10c,13,14b,20] the elliptical porous columns with intracolumnar order reported here differ from them and represent the first examples of noncircular synthetic porous structures that self-organize in periodic arrays. Previous porous structures exhibited only a circular pore shape.[9,10,12]

A strategy to provide a reversible or irreversible change from elliptical to circular pore shape via different thermal treatment was elaborated, and its mechanism was elucidated. The dimensions of the elliptical pore were calculated by developing a method for the reconstruction of the powder XRD patterns of the Φ_{r-c}^{io} lattice. Additional X-ray experiments performed on aligned fibers together with experimental densities, molecular modeling, and the dimensions of the pore were used to perform the complete structural and retrostructural analysis of the elliptical pore. The pore is assembled by a network of dipeptide H-bonds that provides a rigid and ordered intracolumnar structure.[9,10,12] This intracolumnar order resembles that encountered in related biological assemblies[21] and in circular pores.[10b,c] The experiments reported here may facilitate the design of noncircular porous protein mimics and of membranes that are externally regulated and mediate separation processes based on the shape.

Acknowledgment. Financial support by the National Science Foundation (DMR-0102459 and DMR-0548559), the Office of Naval Research, and the P. Roy Vagelos Chair at Penn is gratefully acknowledged.

Supporting Information Available: Experimental Section containing detailed synthesis, structural, and retrostructural analysis. This material is available free of charge via the Internet at http://pubs.acs.org.

JA0611902

(20) (a) Percec, V.; Glodde, M.; Bera, T. K.; Miura, Y.; Shiyanovskaya, I.; Singer, K. D.; Balagurusamy, V. S. K.; Heiney, P. A.; Schnell, I.; Rapp, A.; Spiess, H.-W.; Hudson, S. D.; Duan, H. *Nature* **2002**, *417*, 384−387; for representative reviews containing also examples of columnar rectangular liquid crystals assembled from elliptical columns, see: (b) Bushby. R. J.; Lozman, O. R. *Curr. Opin. Colloid Interface Sci.* **2002**, *7*, 343−354. (c) Tschierske, C. *J. Mater. Chem.* **2001**, *11*, 2647−2671. (d) Binnermans, K. *Chem. Rev.* **2005**, *105*, 4148−4204.
(21) Bernal, J. D.; Fankuchen, I. *Nature* **1937**, *139*, 923−924.